Angle-resolved photoemission extended fine-structure study of the structure of $p(2\times2)$K/Ni(111)

Zhengqing Huang,* L. Q. Wang, A. E. Schach von Wittenau, and Z. Hussain
Department of Chemistry, University of California, Berkeley, California 94720
and Chemical Sciences Division, Mail Stop 2-300, Lawrence Berkeley Laboratory, 1 Cyclotron Road, Berkeley, California 94720

D. A. Shirley
Departments of Chemistry and Physics, Pennsylvania State University, University Park, Pennsylvania 16802
(Received 23 October 1992)

Angle-resolved photoemission extended fine structure (ARPEFS) from the potassium 1*s* core level was measured for the quantitative structural determination of the $p(2\times2)$K/Ni(111) overlayer at 130 K. Our analysis of the ARPEFS $\chi(k)$ curves detected along [111] and [771] showed that the potassium atoms are preferentially adsorbed on the atop sites, in agreement with a previous low-energy-electron-diffraction (LEED) study of the same system. The K-Ni bond length is 3.02±0.01 Å, yielding an effective hard-sphere radius of 1.77 Å for potassium. The first-to-second-layer spacing of nickel is 1.90±0.04 Å, a 6.5% contraction from the bulk spacing of 2.03 Å. Furthermore, the first nickel layer shows neither lateral reconstruction (0.00±0.09 Å) nor vertical corrugation (0.00±0.03 Å). A comparison of the structural parameters with those determined from the LEED study is presented. The limitations of Fourier analysis for site determination and the importance of comparing ARPEFS experimental data with theoretical simulations in both *k* space and *r* space are also discussed.

I. INTRODUCTION

Recently there has been increasing interest in, and controversy over, the structure and bonding of adsorbed submonolayer alkali metals on surfaces.[1–4] Alkali metals have long been known[5] to lower substantially the work function of both metals and semiconductors when adsorbed on these surfaces, and have been widely used in technological applications such as heterogeneous catalysis[6] and thermionic energy conversion.[7] Extensive experimental[1,3,4] and theoretical[2,8,9] work has been undertaken to study the chemical bonding between the adsorbed alkali atoms and the metal substrate. While it has long been held[1] that this bonding is mainly ionic at low coverage due to the charge donation by the strongly electropositive alkali metals, and then becomes more metallic at higher coverage due to the depolarization of the adsorbate dipoles, some recent studies[2,3,9] have suggested that there is no charge transfer at all coverages, and the adsorbate-substrate bonding is better described as covalent at low coverage and metallic at high coverage.[3]

Few complete determinations of the adsorption geometries of the alkali-metal overlayers have been reported, probably due to the relatively complex phase diagrams of these systems, where commensurate structures are usually possible only within small coverage and temperature ranges. Among the structures determined, an interesting trend is that the alkali atoms are found to adsorb on the atop sites for $p(2\times2)$ structures formed at 0.25-monolayer coverage on the close-packed hexagonal surfaces, as demonstrated in the low-energy-electron-diffraction (LEED) studies of $p(2\times2)$Cs/Cu(111) (Ref. 10) and more recently, of $p(2\times2)$Cs/Rh(0001) (Ref. 11) and $p(2\times2)$K/Ni(111) (Ref. 12). These studies also showed that the effective hard-sphere radius (the adsorbate-substrate bond length less the metallic radius of the substrate) of the atop-adsorbed alkali metal is much smaller than its metallic radius. For Cs/Rh(0001), it was found that at the higher coverage of 0.33 monolayer, where the cesium overlayer forms a $\sqrt{3}\times\sqrt{3}R30°$ structure, the Cs atoms are favored to adsorb on the threefold hollow sites and have larger hard-sphere radii (+0.3 Å) than in the $p(2\times2)$ structure. A recent normal-incidence standing x-ray wave-field absorption (NISXW) study[13] of Rb/Al(111), however, showed that the Rb atoms are adsorbed on the top sites and that the Rb-Al bond length does not change (±0.10 Å) over the coverage range 0.12–0.33 monolayers. Again, interpretations of the coverage dependence (or independence) of adsorption site and bond length cover both the ionic-metallic and covalent-metallic bonding models. It appears that the nature of the chemical bonding is a complicated function of the metals involved, the surface-atomic density and symmetry, and the coverage of the alkali atoms. More experimental and theoretical studies are needed to further the understanding of the chemistry of alkali-metal adsorbates on metal surfaces.

In this paper, we report the structural study of the $p(2\times2)$K/Ni(111) surface using angle-resolved photoemission extended fine structure (ARPEFS).[14] Most earlier ARPEFS work has concentrated on atomic overlayers of phosphorus, sulfur, and chlorine on surfaces.[14–17] A recent study of the unusual $p2mg(2\times1)$CO/Ni(110) structure[18] extended the application of ARPEFS to the study of molecules adsorbed on surfaces. It also demonstrated that ARPEFS is capable of determining the structures of more complex systems, in this case a surface layer with two inequivalent molecules in a unit cell and tilted molecules occupying positions that are displaced from high-symmetry sites. The

structural study of the $p(2\times2)$K/Ni(111) surface reported here represents the extension of the ARPEFS technique to the study of yet another type of surface overlayer, the adsorption of metals on other metal substrates. It is important that structural determination of surface overlayers be confirmed by more than one technique. The recent LEED study[12] of the $p(2\times2)$K/Ni(111) adsorption system by Fisher *et al.*, in which the potassium atoms were found to adsorb on atop sites with a rather short K-Ni bond length of 2.82 Å, provides an opportunity for comparison of the structural results for this system.

The ARPEFS technique used in this work has been described in detail elsewhere.[19] A brief summary is given here. In an ARPEFS study, the photoemission partial cross section of a core level (such as the 1*s* level) of the adsorbed atoms is measured in one or more emission directions as a function of the photoelectron kinetic energy in the range of approximately 50–500 eV. Because the photoelectron wave is emitted in all directions (*p* wave for 1*s* electrons), part of the wave will have been scattered by nearby substrate and adsorbate atoms before it reaches the detector. The scattered waves and the unscattered wave undergo interference, either constructively or destructively, depending on their path-length differences and the electron kinetic energy. The interference pattern shows up in the measured energy-dependent photoelectron intensity as peaks and valleys in the otherwise slowly varying atomiclike cross section. This oscillatory part, which contains information about the local geometry of the photoemitting atom, is what constitutes the ARPEFS. Experimental ARPEFS curves could in many simple cases be Fourier transformed to obtain qualitative structural information such as adsorption sites and approximate interatomic distances, while comparison with multiple-scattering spherical-wave (MSSW) calculations is necessary for a quantitative determination of the structure.

The remainder of this paper is organized as follows: Sec. II describes the experiment, in particular the preparation of potassium overlayers and the collection of potassium 1*s* photoemission data. Section III gives a brief account of the procedure used to reduce experimental photoemission spectra into an ARPEFS curve. Section IV describes a detailed analysis of the surface structure and presents optimized structural parameters and their estimated errors. Section V discusses the results of this work and compares them with results from the LEED study.

II. EXPERIMENT

The experiments were performed in an ion-pumped ultrahigh-vacuum chamber with a typical base pressure of 7×10^{-11} Torr. The Ni(111) crystal was cleaned by the standard method of repeated cycles of sputtering and annealing prior to this work. Laue backscattering verified its orientation to be within $\pm1°$ of the (111) plane. The crystal was then spot welded between two tungsten wires onto a tantalum plate that was mounted on a high-precision manipulator equipped with a liquid-nitrogen cooling system. The temperature of the crystal was measured using a chromel-alumel thermocouple spot welded to the tantalum plate very close to the Ni crystal. The readings of the thermocouple were calibrated at higher temperatures using an optical pyrometer. Routine sample cleaning was done by sputtering with a 500–1000 eV Ar^+ beam and annealing at 800–1000 K with electron-beam bombardment from behind the crystal. To remove the carbon contaminant more effectively, the sample was occasionally exposed to 1–5 L of O_2 at room temperature before the annealing. The surface was considered clean when LEED showed a sharp (1×1) pattern with little background, and Auger electron spectroscopy (AES) revealed no impurities.

Potassium was evaporated onto the Ni(111) surface from commercial alkali-metal dispensers (SAES Getters). A shutter installed in front of the source provided accurate timing of potassium evaporation. Each source was outgassed at a current of 3–4 A for two to three days. During this period, the source was also brought to gradually higher current (up to the operating current of ~6–6.5 A for potassium deposition) briefly until the pressure inside the chamber did not rise by more than 1×10^{-10} Torr during evaporation. Relative coverage was assumed to be proportional to evaporation time, while the absolute coverage was calibrated to the evaporation time required to produce the $p(2\times2)$ LEED pattern that should appear at 0.25 monolayer (one potassium atom for every four surface Ni atoms). This work was mainly concerned with the commensurate $p(2\times2)$ structure, and evaporation was stopped when a low-background, sharp $p(2\times2)$ LEED pattern appeared. The Ni(111) substrate was held at room temperature during potassium deposition. The crystal was then cooled to ~130 K for low-temperature measurements.

An ARPEFS experiment involves detecting the angle-resolved photoelectron intensity of a certain atomic core level (potassium 1*s* level in this study) as a function of electron kinetic energy in one or more directions. Therefore a variable-energy vacuum ultraviolet or x-ray source is required. These experiments were conducted on beamline X24A at the National Synchrotron Light Source at Brookhaven National Laboratory. X-ray photons from the storage ring were monochromatized using a Si(111) double-crystal assembly and focused onto the sample by a toroidal nickel-coated quartz mirror. ARPEFS curves were measured at 130 K along two emission directions, the surface normal [111] and 30° from [111] toward [11$\bar{2}$]. The off-normal direction is very close to [771] (29.5° from [111] toward [11$\bar{2}$]), and will for simplicity be denoted as such hereafter. The photon polarization directions were along [771] for both the [111] and [771] curves. These two experimental geometries, along with a model of the $p(2\times2)$K/Ni(111) structure, are illustrated in Fig. 1.

For each of the two geometries described above, the potassium 1*s* photoemission spectra were measured in increments of 0.08 $Å^{-1}$ (corresponding to 3–6 eV, depending on the kinetic energy) over the kinetic-energy range of approximately 70–370 eV (the photon energy in the range of 3070–3370 eV). Each photoemission spectrum had an energy window of 25–30 eV, with the photopeak

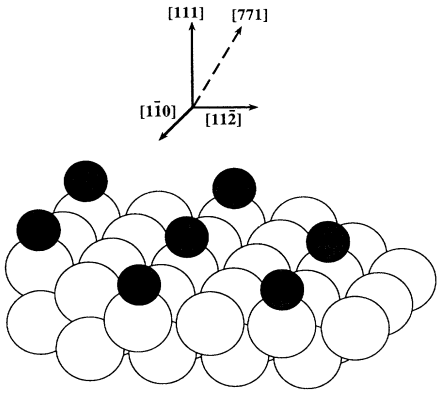

FIG. 1. The $p(2\times2)$K/Ni(111) surface is shown, with the potassium atoms occupying the atop sites. The emission directions in which the electrons are detected are labeled [111] and [771]. The photon polarization directions are along [771] for both experimental geometries. For ease of viewing, the potassium atoms (shaded) are reduced.

appearing approximately at the center. Data were collected using an angle-resolved and rotatable electrostatic hemispherical analyzer operating at 160-eV pass energy. The angular resolution (half-solid angle) of the input lens is 3°. The combined resolution of the photon source and the electron-energy analyzer was around 2.0 eV throughout the energy range of this experiment. Each ARPEFS curve entailed about 3 h of measurement. The major contaminants were carbon and oxygen, whose coverages were estimated to be less than 0.04 monolayer at the end of the measurement of each ARPEFS curve. As the kinetic energy of the potassium 1*s* electrons was scanned across the carbon *KLL* Auger lines near 275 eV, about three-quarters into the measurement of an ARPEFS curve, no detectable carbon Auger peaks were observed. This provided additional evidence that the level of impurities on the surface was quite low during the experiment.

III. DATA REDUCTION

To generate photoemission partial cross sections as a function of photoelectron kinetic energy, it is necessary to extract the photopeak areas of all spectra for a given geometry and normalize these areas to one another in order to compensate for the variations in the energy-dependent photon flux and the transmission function of the electron analyzer. Details of this procedure have been described elsewhere.[18] In brief, each photoelectron spectrum was least-squares fitted using a Gaussian-convoluted Doniach-Šunjić function,[20] a Gaussian-convoluted step function, and an experimentally determined background template. These functions modeled the photoemission peak, the energy-loss function, and the inelastic background, respectively. The background template also served as an excellent normalization scheme and was also used to subtract the potassium *LMM* Auger peaks from the photoelectron spectra in which these Auger features appeared.

Once the photoelectron spectra were fitted with the above-mentioned functions, the energy-dependent photoemission intensity $I(E)$ was generated by plotting the Doniach-Šunjić peak area, divided by the coefficient of the background template, as a function of the mean energy of the peak. $I(E)$ can be described by

$$I(E)=I_0(E)[1+\chi(E)] , \tag{1}$$

where $I_0(E)$ is a slowly varying atomiclike partial photoemission cross section for potassium 1*s*, and $\chi(E)$ is the rapid oscillation of this cross section due to the scattering of electrons by nearby atoms. $\chi(E)$ is the ARPEFS and can be obtained from $I(E)$ by the removal of $I_0(E)$,

$$\chi(E)=[I(E)/I_0(E)]-1 . \tag{2}$$

$I_0(E)$ is the potassium 1*s* atomic cross section modified by the change of chemical environment upon adsorption to the Ni surface. Experimentally, it could also include other low-frequency variations resulting from our data collection and reduction procedures. Therefore a low-order polynomial was used to least-squares fit $I(E)$ and then used as an approximation to $I_0(E)$. This procedure was shown[18] to reproduce $\chi(E)$ curves very well, except for the ARPEFS oscillations that come from those scattering events with path-length differences of less than around 2 Å, which could be distorted or eliminated depending on the choice of the particular polynomial. Since the path-length differences were much larger than 2 Å for all the structural models that we considered in this study, this method of $I_0(E)$ extraction did not cause any significant errors in the derived $\chi(E)$ curves.

Having extracted the ARPEFS $\chi(E)$ curves, it is necessary to convert $\chi(E)$ into $\chi(k)$ for Fourier analysis, where k is the magnitude of the photoelectron wave vector in-

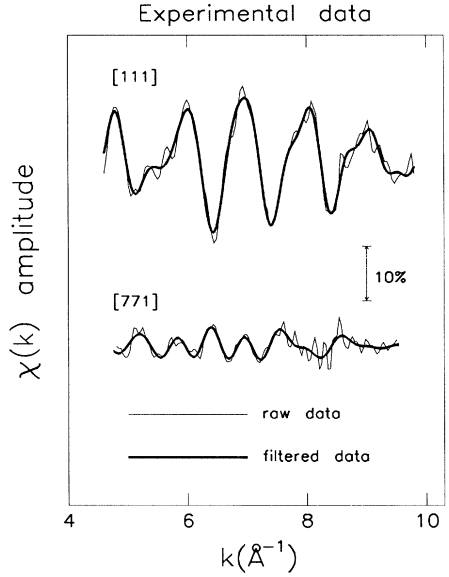

FIG. 2. Experimental $\chi(k)$ curves. The path-length-difference cutoffs for the filtered data are 2–15 Å for both [111] and [771] curves. The [111] curve is the average of two curves, each measured on a newly prepared potassium overlayer.

side the Ni crystal, and can be calculated using the de Broglie relation

$$k(\text{Å}^{-1})=0.5123[E+V_0(\text{eV})]^{1/2}\ , \tag{3}$$

where V_0 is the inner potential of the solid. The exact value of V_0 is not known, but is around 10 eV for nickel, possibly a few eV less after the adsorption of potassium due to the lower work function. V_0 is treated as an adjustable parameter in our R-factor analysis; for the purpose of qualitative Fourier analysis, we simply used 8 eV to do the conversion. The ARPEFS $\chi(k)$ curves obtained in this manner are illustrated in Fig. 2. The [111] $\chi(k)$ curve represents the average of two separate runs on separately prepared potassium overlayers. The [771] $\chi(k)$ curve was also measured on a newly prepared overlayer.

IV. RESULTS AND ANALYSIS

This section is divided into two parts. Section IV A presents procedures and results of detailed structural analysis using the [111] data. The [771] curve has very small oscillations and was not used to search for the structure. It will be presented in Sec. IV B as supporting evidence for the atop-site adsorption geometry that was favored from the analysis of Sec. IV A. In Sec. IV C, we discuss the results of structural refinements for the atop site with consideration to the possibility of surface reconstructions, and present estimates of uncertainties associated with the optimized structural parameters.

A. The [111] data

Recent ARPEFS studies[15–18] have employed a two-step approach to the surface structural determination using the measured $\chi(k)$ curves. Adsorption sites and approximate interatomic distances could in many cases be determined from simple Fourier analysis, while quantitative surface geometries require theoretical simulations. To understand how structural information can be extracted from the ARPEFS $\chi(k)$ curves, it is useful to examine the ARPEFS equation, which in the limit of single scattering follows the expression

$$\chi(k)=2\sum_j \frac{\cos\beta_j}{\cos\gamma}\frac{|f(\theta_j)|}{r_j}\cos[kr_j(1-\cos\theta_j)+\phi_j] \times e^{-\Delta R_j/\lambda}e^{-\sigma_j^2(1-\cos\theta_j)k^2}\ , \tag{4}$$

where j indexes all atoms near the potassium atom from which the 1s core-level photoemission is measured. The angle β_j is between the photon polarization vector and the vector connecting the photoemitting potassium atom and the jth scattering atom; γ is the angle between the polarization and the electron emission directions; and r_j is the interatomic distance between the photoemitter and the jth surrounding atom. The emission-angle-dependent path-length difference is given by $\Delta R_j=r_j(1-\cos\theta_j)$, where θ_j is the scattering angle. The k-dependent complex scattering factor $f(\theta_j)$ represents the jth atom in the scattering problem, and can be decomposed into the amplitude $|f(\theta_j)|$ and the phase ϕ_j. It is well known that the scattering amplitude $|f(\theta_j)|$ is strongly peaked in the forward-scattering ($\theta_j=0°$) and backscattering ($\theta_j=180°$) directions, with backscattering followed by forward scattering (double scattering) having the largest combined amplitude. Surface thermal vibrations are described using a correlated Debye-Waller model[21] and represented in Eq. (4) by $e^{-\sigma_j^2(1-\cos\theta_j)k^2}$, where σ_j^2 is the mean-square relative displacement (MSRD) between the photoemitter and the jth scattering atom, projected on the photoelectron momentum change direction. The inelastic losses due to the excitation of plasmons and electron-hole pairs by the energetic photoelectrons are described empirically by an exponential decay factor $e^{-\Delta R_j/\lambda}$, where λ stands for the electron mean free path.

1. Fourier analysis

The sinusoidal form of $\chi(k)$ in Eq. (4) suggests that if a Fourier transformation is made of the data, the positions of the peaks in the Fourier transform should appear near the path-length differences $\Delta R_j=r_j(1-\cos\theta_j)$, shifted by some small amount due to the scattering-phase function ϕ_j. The shift caused by ϕ_j is usually less than 0.2 Å and can be ignored for qualitative analysis. In systems where different adsorption sites yield significantly different path-length differences, usually only one of the possible sites considered would have path-length differences that match the Fourier peak positions within a physically reasonable range for the adsorbate-substrate bond length. In addition, the intensities of the Fourier peaks should also reflect the influence of the various terms in Eq. (4), especially the strong dependence of the scattering amplitude on the scattering angle. A good match of peak positions and relative intensities provides the basis for the selection of a favored site.

The Fourier-transform spectrum for the [111] $\chi(k)$ curve (Fig. 2) is shown in Fig. 3. The dominant feature around 6 Å is mainly associated with electrons being scattered from first-layer nearest-neighbor nickel atoms directly (or nearly directly) under the potassium atoms along [111]. Since the resolution of the Fourier spectrum is ~2 Å, and the 6-Å peak is broad and asymmetric, it

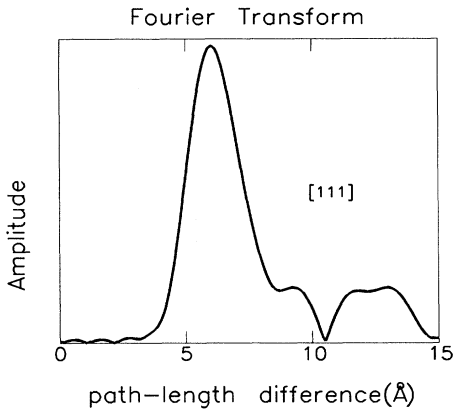

FIG. 3. The Fourier transformation of the [111] $\chi(k)$ curve pictured in Fig. 2.

could actually be the overlap of two or more closely spaced peaks. It can be shown that, for the various potassium adsorption sites that we shall consider, namely the atop site, the hcp and fcc hollow sites, and the bridge site, scattering of photoelectrons by the next-nearest-neighbor first-layer nickel atoms could make a small contribution to the broad 6 Å, with a path-length difference of ~7 Å. However, the major contribution is from the strong scattering at ~6 Å, and the following discussion should not be affected by the smaller contribution at 7 Å. The much weaker second peak at ~9.3 Å is at least partly attributable to backscattering (or near backscattering) from the nearest second-layer nickel atoms. Because of the close packing of the Ni(111) surface and the large size of the potassium atoms, it is possible for all the adsorption sites considered to match path-length differences determined from the experiment within a physically reasonable range of K-Ni bond lengths. However, because in the case of atop adsorption the potassium atom has a first-layer nickel atom directly underneath along the [111] surface normal, and the second-layer nickel atoms lie at angles somewhat removed from the backscattering (followed by forward-scattering) geometry, Fourier transform of the [111] $\chi(k)$ curve should show a large intensity ratio ($I_{6\text{ Å}}/I_{9.5\text{ Å}}$) of the resulting two peaks. For the other candidate sites, this intensity ratio is expected to be smaller. Therefore, the large intensity ratio of these two peaks in the experiment results alone would seem to favor the atop site. However, since factors other than the scattering angle, such as the number of scattering atoms, thermal vibrations, and the distances of scattering atoms from emitter [Eq. (4)] can also affect the overall intensity of a peak, the above analysis alone does not exclude the other sites, especially considering that the scattering angles for the other sites are not too far away from the backscattering or forward-scattering conditions. To distinguish among the various sites, a more quantitative knowledge of how these various factors affect the scattering process is required. For this we will use an *R*-factor minimization procedure based on theoretical multiple-scattering spherical-wave (MSSW) simulations.

2. *MSSW analysis*

The theoretical background of the MSSW has been described in great detail elsewhere.[21] It can be simplified to Eq. (4), but the MSSW is a much more complete and complicated theory that correctly takes into account, among other things, multiple-scattering and spherical-wave effects to numerically calculate $\chi(k)$. A MSSW calculation requires a set of trial *structural* parameters, such as adsorption site(s), atomic interlayer spacings, and surface reconstruction and corrugation, as well as *nonstructural* parameters that include atomic partial-wave phase shifts (PWPS), isotropic Debye temperatures of surface atomic layers, photon polarization and electron detection directions, analyzer aperture, mean free path parameters, and experimental temperature. Values of some of the parameters are varied to calculate a series of $\chi(k)$ curves, which are then compared with the experimentally determined $\chi(k)$ curves. Typically one structure gives the best agreement between theory and experiment, and can be taken as the most likely structure.

In the present study, five different adsorption sites were evaluated for the geometric structures of the potassium overlayer. In addition to the above-mentioned atop site, fcc hollow site, hcp hollow site, and bridge site, we also included the substitutional site, in which one out of every four first-layer nickel atoms is replaced by a potassium atom while still preserving the $p(2\times2)$ superlattice symmetry. Only two structural parameters, namely the potassium-nickel interatomic distance and the first- to-second-nickel-interlayer spacing, were varied in the initial search. Their ranges are 2.5–3.7 and 1.75–2.3 Å, respectively. For the bridge-site adsorption, the $\chi(k)$ curves for three domains were calculated and averaged.

Among the nonstructural parameters, only the potassium surface Debye temperatures and the inner potential were varied. The nickel bulk Debye temperature was fixed at 375 K, while the surface Debye temperature was fixed at 265 K, which assumes that the mean-square relative displacement of the surface nickel atoms is twice that of the bulk. The horizontal and vertical Debye temperatures for the potassium layer were varied independently between 50 and 300 K. The inner potential V_0 in Eq. (3), used to convert experimental data from the energy space into k space for comparison with theory, was treated as an adjustable parameter and allowed to vary between 4 and 12 eV.

The nickel and potassium partial-wave phase shifts used in the present study were calculated using a modified program by Pendry,[22] with the atomic scattering potentials taken from the calculations of Moruzzi, Janak, and Williams.[23] A total of 20 phase shifts were calculated. The nickel-phase shifts derived in this manner were the same as those in previous studies.[24,18] The inelastic scattering was accounted for by including an exponential factor $e^{-r/\lambda}$ in the scattering amplitude, where $\lambda=ck$, and $c=0.753$. The aperture size of the hemispherical electron analyzer was fixed at 3° half angle. The photon polarization and electron detection directions, and the crystal temperature (130 K) were experimentally determined quantities. Although they could also be varied in the calculations, they were set at their experimental values to avoid a cumbersomely large parameter set.

To determine the geometric structure from the ARPEFS data, the experimental $\chi(k)$ curve was compared with MSSW calculations by varying the values of the above-mentioned five structural and nonstructural parameters until the best agreement was reached. This optimization was implemented by minimizing the R factor, defined as

$$R=\frac{\sum_i [\chi_E(k_i)-\chi_T(k_i,\{P_j\})]^2}{\sum_i \chi_E^2(k_i)}, \tag{5}$$

where $\chi_E(k)$ is the experimentally determined ARPEFS curve, $\chi_T(k)$ is the MSSW calculation, subscript i indicates the ith data point, and $\{P_j\}$ is the set of parameters to be optimized. The k range was 4.8–9.7 Å^{-1}. To min-

imize the R factors for each of the five trial structures, a simplex routine was used to search automatically both the structural and nonstructural parameters simultaneously until a minimum R factor was reached. Different initial guesses were tried to make sure that results from the fits were reproducible.

The experimental $\chi_E(k)$ curve used in the R-factor minimization was smoothed by Fourier filtering out high-frequency noise. Residual low-frequency contributions not removed by the $I_0(E)$ extraction procedure described in Sec. III were also filtered out. The cutoff range was 2–15 Å. The theoretical $\chi(k)$ curves were calculated for path-length differences between zero and 15.5 Å, then filtered at 2–15 Å, as was the experimental curve.

The structural and nonstructural parameters determined from the best fits for the five test sites are summarized in Table I. Comparison between the experimental and theoretical $\chi(k)$ curves is presented in Fig. 4. Table I shows that the agreement between experiment and theory is best for the atop site, with the lowest R factor, though the R factors for the fcc and hcp sites are not too bad. This can also be seen in Fig. 4, where the experimental and the theoretical $\chi(k)$ curves have the best visual match for the atop site, but for the fcc and the hcp sites the match in the gross peak positions [but not in the $\chi(k)$ amplitudes] is also reasonable. However, if we Fourier transform all the above best-fit theoretical $\chi(k)$ curves and compare them with the experimental curve, as shown in Fig. 5, it is clear that the atop site stands out as having a much better match between theory and experiment in both the Fourier-peak positions and the relative amplitudes of these peaks. Since the determination of the adsorption site relies in large part on the first and second peaks, the superior agreement for the atop site provides strong evidence that it is the most probable site for potassium.

One might ask why the fits for the other (than atop) sites look better in k space (Fig. 4) than in r space (Fig. 5), especially since the k-space data are usually thought to contain more information. A possible explanation is that in the k-space fitting, many scattering events (from first layer, second layer, etc.) combine to make the total set of frequency, phase, and amplitude parameters. For the fcc, hcp, bridge, and substitutional sites, the relative contribution from the second layer is quite important (as can be seen from the strong Fourier peak near 10 Å in the calculated curves). They can combine with the less important (compared with the atop-site) contribution from the first layer to make the overall fit look reasonable. On the other hand, if we were to do the R-factor analysis using the Fourier transform of the experimental and theoretical curves (i.e., in r space), it is conceivable that the fit for these sites could be improved, but the optimized structural parameters for all but the atop site would be quite different from those obtained from the k-space fit. Therefore it is very important to Fourier transform the best-fit $\chi(k)$ curves and compare them in the r space, especially when the k-space fit does not strongly favor a particular site. In summary, while the k-space R-factor minimization aims to fit the overall phase, amplitude, and frequency of a calculated $\chi(k)$ curve with those of an experimental $\chi(k)$ curve, the Fourier transform decomposes the $\chi(k)$ curves into individual frequencies corresponding to scattering path-length differences and allows us to examine whether each frequency is well represented in the $\chi(k)$ curves. Good experimental-theoretical agreement in both k and r spaces enhances the confidence for selecting a given parameter set (including adsorption site) over the others.

B. The [771] data

Additional evidence for atop-site adsorption can be obtained from the off-normal [771] $\chi(k)$ curve. Ideally we could have applied the above R-factor minimization to this $\chi(k)$ curve to obtain another set of optimized structural and nonstructural parameters, which would have allowed us to verify if consistent results were obtained from independent measurements. In cases where only one of the tested sites has consistent results and also has the lowest R factors, such as in the case of $p2mg(2\times1)$CO/Ni(110) (Ref. 18), one can say with confidence that the preferred site is correct. The independently determined sets of parameters also provide a more meaningful mechanism for the estimation of errors. In the present study, however, the small oscillations and the rather large relative uncertainties (±3.5% maximum oscillations vs 2% uncertainty) in the experimental [771] $\chi(k)$ curve could either make the R-factor optimization nonconvergent, or they could translate into large error bars for the structural parameters. Our approach was instead to calculate theoretical [771] $\chi(k)$ curves using the optimized parameters (Table I) for each of the five trial sites from the [111] data and compare these calculated $\chi(k)$ curves with the experimental curve. Figure 6 shows the results. Again, due to the small oscillations and the

TABLE I. Optimized parameters obtained from the R-factor minimization for the various tested adsorption sites.

Adsorption site	K-Ni bond length (Å)	Ni(1)-Ni(2) distance (Å)	Debye temperature of potassium (K) horizontal	vertical	Inner potential (eV)	R-factor
substituted	3.60	1.99	105	265	4.0	0.62
bridge	3.20	1.96	60	275	7.9	0.36
hcp hollow	3.27	2.01	60	200	4.0	0.32
fcc hollow	3.26	1.94	85	175	7.7	0.31
top	3.02	1.90	75	175	6.6	0.21

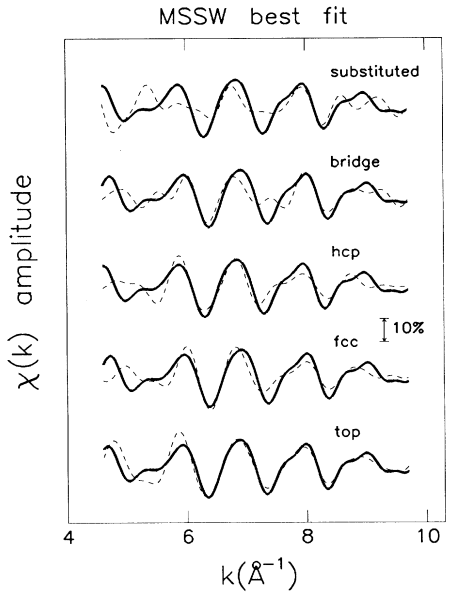

FIG. 4. A comparison between the [111] experimental $\chi(k)$ curve and best-fit MSSW calculations for the various trial adsorption sites. The solid lines are experimental curves and the dashed lines are MSSW calculations. The $\chi(k)$ functions oscillate around a mean value of zero by $\sim\pm 10\%$ maximum amplitude, shown to scale. The structural and nonstructural parameters used to generate the theoretical curves are listed in Table I. Experimental curves do not line up exactly for the different sites because the optimized inner potentials are different [Eq. (3)].

large error bars, what we will focus on here is not the point-by-point fit of the curves, but the overall agreement in the peak and valley positions and the overall magnitude of the oscillations. From Fig. 6, we see that the experimental-theoretical agreement is very poor for the substitutional site and the fcc and hcp hollow sites. If the potassium atoms were to occupy one of these sites, the large oscillations in the $\chi(k)$ curves (6–10 %) as modeled by the MSSW theory should have shown up in the experimental $\chi(k)$ curve as well, even given the large error bars. The match in peak positions for these sites was also quite poor. For the atop and bridge sites, the experimental-theoretical fits are about equally good, but for atop-site adsorption the match in the peak positions is significantly better, with the largest deviation coming in the low-k range, where the MSSW theory is less accurate.

C. Structural refinement and error analysis

Combining the results of Secs. IV A and IV B, we conclude that the potassium atoms are strongly favored to adsorb on the atop sites in the $p(2\times 2)$K/Ni(111) surface layer. We have also determined that the K-Ni bond length is 3.02 Å and the first- to-second-layer spacing of nickel is 1.90 Å, or about a 6.5% contraction from the bulk spacing of 2.03 Å. In this section, we will explore the possibility that the surface layer may arrange itself in more complicated ways. In particular, we will consider whether, in the $p(2\times 2)$ superlattice, in which only one out of every four first-layer nickel atoms is directly bonded to a potassium atom and the other three do not have direct bonding with potassium, the first-layer nickel atoms without the potassium bonding may undergo

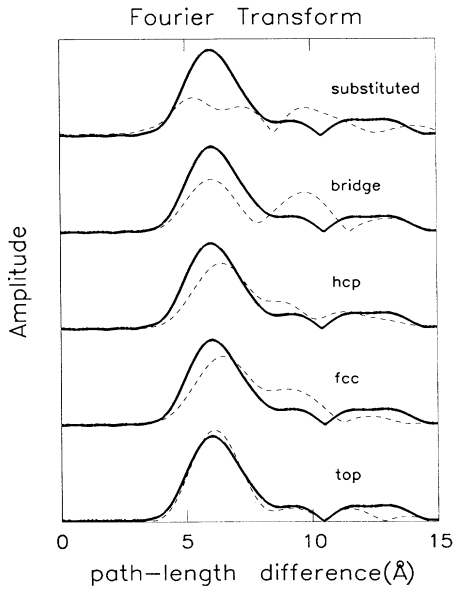

FIG. 5. The Fourier transformation of the $\chi(k)$ curves in Fig. 4. The solid lines are experimental data and the dashed lines are MSSW calculations.

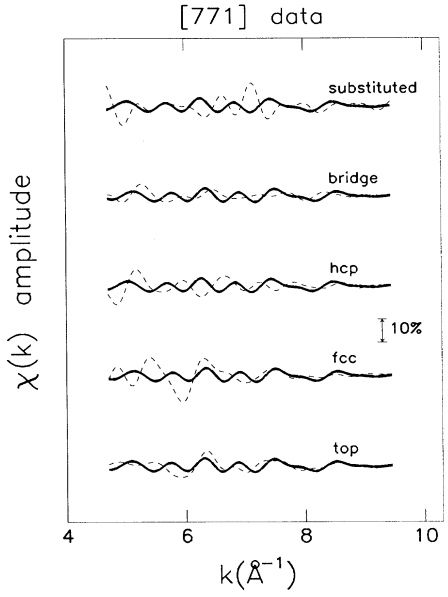

FIG. 6. A comparison between the [771] experimental $\chi(k)$ curve and the MSSW calculations for the various trial adsorption sites. The solid lines are experimental curves and the dashed lines are MSSW calculations. The structural and nonstructural parameters used to generate the theoretical curves are those of the best-fit results using the [111] curve (Table I).

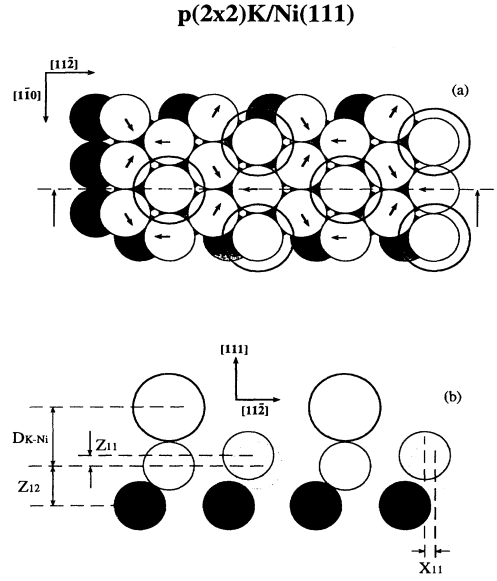

FIG. 7. (a) Top and (b) side views of $p(2\times2)$K/Ni(111), showing the vertical and lateral reconstruction of the first-layer nickel atoms. The larger open circles represent potassium atoms, the smaller open circles the first-layer nickel atoms, and the shaded smaller circles the second-layer nickel atoms. The structural parameters used in the final R-factor minimization are defined in the side view. The light circles seen in the side view denote first-layer nickel atoms in the unreconstructed geometry.

reconstructions both in the vertical and lateral directions, while at the same time preserving the $p(2\times2)$ symmetry. These possible reconstructions are illustrated in Fig. 7.

We searched the optimal values of the lateral and vertical displacements of these nickel atoms using the [111] $\chi(k)$ curve and the above-mentioned R-factor minimization in two ways: by varying these two parameters while fixing the other parameters at their previously optimized values (Table I), and by varying all the parameters at the same time. In both cases, we found little reconstruction (<0.01 Å) of the first-layer nickel, and the R factor was not improved either. In the second method, the other parameters were also found to change little (<0.01 Å, 5 K, and 0.6 eV for distances, Debye temperatures, and the inner potential, respectively) from those values in Table I. Therefore, we conclude that the surface does not reconstruct upon the adsorption of potassium, except for the downward shift of the first- to-second-layer nickel spacing from the bulk value.

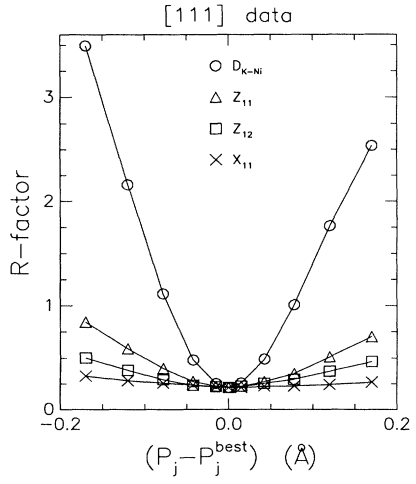

FIG. 8. Plots of the R factor vs the deviation $(P_j-P_j^{best})$ of parameter j from its optimized value P_j^{best} for the four structural parameters defined in Fig. 7. Note the large R-factor range of the ordinate.

TABLE II. Best-fit structural parameters and statistical errors (in parentheses) from this work and the LEED study, Ref. 12.

Source	D_{K-Ni} (Å)	Z_{12} (Å)	Z_{11} (Å)	X_{11} (Å)
ARPEFS	3.02 (0.01)	1.90 (0.04)	0.00 (0.03)	0.00 (0.09)
LEED	2.82 (0.04)	1.90 (0.03)	0.12 (0.02)	0.06 (0.06)

To estimate the uncertainty associated with each of the structural parameters that were varied (the K-Ni bond length D_{K-Ni}, the vertical distance between the potassium-covered first-layer nickel and the second-layer nickel Z_{12}, and the vertical displacement Z_{11} and lateral displacement X_{11} between the occupied and unoccupied nickel atoms in the first layer), we calculated how the R-factor changes when these parameters are varied around their optimal values. Figure 8 plots the R factor versus the deviation $(P_j-P_j^{best})$ of parameter j from its optimized value P_j^{best}. All parameters except the abscissas were fixed at their optimal values obtained from the above-mentioned "second" method, in which all parameters were changed at the same time. What we observe in Fig. 7 is that the R factor—hence the $\chi(k)$ curve—is much more sensitive to the change in the K-Ni distance, with a well-defined, steep R-factor minimum, and less sensitive to the other three parameters, particularly the lateral reconstruction X_{11}. The statistical error associated with each parameter can be estimated from the curvature of these R-factor plots using a previously described method.[18,25] Table II lists estimated errors, along with the final optimized values of these parameters. The varying degree of uncertainties for the various parameters is consistent with the observation of the dominant Fourier peak (Fig. 3) attributable to the backscattering from the occupied nickel atoms. The large uncertainty of the lateral displacement (±0.09 Å) as compared to that of the vertical displacement (±0.03 Å) is in large part the result of the strong horizontal thermal vibrations (low Debye temperature) of the potassium surface layer. It underscores the "high" surface mobility (frustrated translations) of adsorbed species on smooth surfaces such as Ni(111), especially for large adsorbates such as alkali metals. In the case of atop adsorption, this thermal motion is even more important because the interaction of the adsorbate with the substrate atoms is much smaller in the lateral direction than in the vertical direction, where there is a strong direct bonding. The low Debye temper-

ature in the lateral direction also helps to explain why the [771] $\chi(k)$ curve has very small oscillations: In addition to the absence of a backscattering nickel atom directly behind the photoemitting potassium atom in the [771] direction, the large lateral thermal vibrations have a greater projection on the off-normal direction [771] than on the normal direction [111] for scattering angles close to 180°. Accordingly, the [771] $\chi(k)$ curve is attenuated more severely by the thermal vibrations [see Eq. (4)].

V. DISCUSSION AND CONCLUSIONS

Our result that the potassium atoms are favored to adsorb on the atop sites in the $p(2\times2)$K/Ni(111) overlayer agrees with the LEED study of Fisher *et al.*, but there are some discrepancies in the final structural parameters. Table II compares the optimized structural parameters from the two studies. Both the LEED and the present ARPEFS studies show that the vertical spacing between the potassium-covered first-layer nickel and second-layer nickel Z_{12} is 1.90 Å, or about a 0.13-Å contraction from the bulk value. The agreement in the horizontal displacement X_{11} is also reasonable, given the large error bars of both studies. However, the K-Ni bond length of 3.02 ± 0.01 Å determined from this study is 0.2 Å larger than the 2.82 ± 0.04 Å obtained by LEED. Another discrepancy is that the ARPEFS study finds no corrugation ($Z_{12}=0.00\pm0.03$ Å) of the first nickel layer, while from the LEED work the first-layer nickel atoms not occupied by potassium atoms are raised by 0.12 ± 0.02 Å outward (toward the vacuum) relative to those that are covered. It should be pointed out that the errors quoted in Table II for this work only include *statistical* errors from the least-square *R*-factor minimization. Other possible sources of error, such as the calculated scattering-phase shifts used in the MSSW simulation and the alignments of the crystal and electron analyzer, may increase the uncertainty of the measured K-Ni bond length by about 0.03 Å, but they still cannot account for the 0.2-Å difference. Sizable differences in the structural results obtained from different techniques have also been reported on other surfaces. For example, studies[26–28] of $p(2\times2)$S/Ni(111) using LEED, ARPEFS, and SEXAFS (surface-extended x-ray-adsorption fine structure) yielded S-Ni bond lengths ranging from 2.10 to 2.23 Å. For some other systems, the structural results are quite consistent among the various techniques. In the case of $c(2\times2)$S/Ni(100), the S-Ni bond length varies only by 0.04 Å (between 2.19 and 2.23 Å) among LEED, ARPEFS, and SEXAFS studies.[29,14,30] It is not clear what the causes are that the K-Ni bond length differs by 0.2 Å between the LEED study of Fisher *et al.* and this work. A SEXAFS experiment on $p(2\times2)$K/Ni(111) may help resolve this difference.[31]

The effective hard-sphere radius of potassium from this work is 1.77 Å; in comparison, the metallic radius of potassium is 2.38 Å. Therefore it appears that the bonding between potassium and nickel is not likely to be purely metallic: we do not expect to see a change of 0.6 Å in the sum of their metallic radii if both the initial and final states are metallic. However, a downshift of the interatomic distance is expected if the K-Ni bond is partly ionic or covalent. A simple explanation is that in the case of covalent bonding the two atoms are pulled closer by the overlapping bonding electrons, while in the case of ionic bonding the ionic radius of potassium is much smaller than its metallic radius. For sixfold-coordinated potassium ions, the radius is around 1.33 Å; it is 0.83 Å for on-top K^+ after correcting for coordination numbers.[32] On the other hand, in the case of ionic bonding, one might reasonably assume that the charge transfer to the nickel atoms will increase their radii by some amount. It is clear that the distinction between ionic and covalent bonding requires more than knowing the bond length. In their Cs/Ru(0001) paper[11] Over *et al.* suggested that the atop sites are favored in the $p(2\times2)$ structure because the substrate atoms between neighboring adatoms in the $p(2\times2)$ structure enhance the screening between the Cs-Ru dipoles. Their observation of the buckling of the first Ru layer ($Z_{11}>0$) seems to support this explanation. Since $Z_{11}=0.00\pm0.03$ Å from this work, it is possible that the quantitative details of the K-K and K-Ni interactions are somewhat different from the Cs-Cs and Cs-Rh interactions, or that the K-Ni bond is somewhat covalent—after all, the bonding is quite directional for on-top adsorption. More experimental and theoretical work is needed to achieve a better understanding of the bonding between adsorbed alkali metals and substrate metals. What may be implied from the structural studies done so far on alkali metals adsorbed on metal surfaces is that, regardless of the bond character, the energy difference between the atop site and the hollow sites is so small because of the smoothness of the close-packed (111) surfaces and the large size of the alkali metals, so that other factors, such as the specific alkali metal and substrate metal involved, and their relative electronegativity, may tip the balance in favor of one of the possible sites.

ACKNOWLEDGMENTS

This work was supported by the Director, Office of Energy Research, Office of Basic Energy Sciences, Chemical Sciences Division of the U.S. Department of Energy under Contract No. DE-AC03-76SF00098. The experiments were performed at the National Synchrotron Light Source at Brookhaven National Laboratory, which is supported by the U.S. Department of Energy's Office of Basic Energy Sciences. We thank D. Lindle and B. Karlin for their assistance at NSLS.

*Present address: The James Franck Institute, The University of Chicago, 5640 South Ellis Avenue, Chicago, IL 60637.

[1] *Physics and Chemistry of Alkali Metal Adsorption,* edited by H. P. Bonzel, A. M. Bradshaw, and G. Ertle (Elsevier, Amsterdam, 1989).

[2] H. Ishida and K. Terakura, Phys. Rev. B **38**, 5752 (1988); H. Ishida, *ibid.* **39**, 5492 (1989); H. Ishida, Surf. Sci. **242**, 341 (1991).

[3]D. M. Riffe, G. K. Wertheim, and P. H. Citrin, Phys. Rev. Lett. **64**, 571 (1990).
[4]G. M. Lamble, R. S. Brooks, D. A. King, and D. Norman, Phys. Rev. Lett. **61**, 1112 (1988).
[5]I. Langmuir, J. Am. Chem. Soc. **54**, 2798 (1932); I. Langmuir and J. B. Taylor, Phys. Rev. **40**, 464 (1932); **44**, 423 (1933).
[6]R. Schlögl, in Ref. 1.
[7]G. N. Hatsopoulos and E. P. Gyftopoulos, *Thermionic Energy Conversion* (MIT Press, Cambridge, MA, 1977).
[8]N. D. Lang, in Ref. 1.
[9]E. Wimmer, A. J. Freeman, J. R. Hiskes, and A. M. Karo, Phys. Rev. B **28**, 3074 (1983).
[10]S. Å. Lindgren, L. Walldén, J. Rundgren, P. Westrin, and J. Neve, Phys. Rev. B **28**, 6707 (1983).
[11]H. Over, H. Bludau, M. Skottke-Klein, G. Ertle, W. Moritz, and C. T. Campbell, Phys. Rev. B **45**, 8638 (1992).
[12]D. Fisher, S. Chandavarkar, I. R. Collins, R. D. Diehl, P. Kaukasoina, and M. Lindroos, Phys. Rev. Lett. **68**, 2786 (1992).
[13]M. Kerkar, D. Fisher, D. P. Woodruff, R. G. Jones, R. D. Diehl, and B. Cowie, Phys. Rev. Lett. **68**, 3204 (1992).
[14]J. J. Barton, C. C. Bahr, S. W. Robey, Z. Hussain, E. Umbach, and D. A. Shirley, Phys. Rev. B **34**, 3807 (1986).
[15]L. J. Terminello, X. S. Zhang, Z. Q. Huang, S. Kim, A. E. Schach von Wittenau, K. T. Leung, and D. A. Shirley, Phys. Rev. B **38**, 3879 (1988).
[16]L. J. Terminello, K. T. Leung, Z. Hussain, T. Hayashi, X. S. Zhang, and D. A. Shirley, Phys. Rev. B **41**, 12 787 (1990).
[17]L. Q. Wang, Z. Hussain, Z. Q. Huang, A. E. Schach von Wittenau, D. W. Lindle, and D. A. Shirley, Phys. Rev. B **44**, 13 711 (1991).
[18]Z. Q. Huang, Z. Hussain, W. T. Huff, E. J. Moler, and D. A. Shirley (unpublished).
[19]J. J. Barton, Ph.D. thesis, University of California, Berkeley, 1985.
[20]S. Doniach and M. Šunjić, J. Phys. C **3**, 285 (1970).
[21]J. J. Barton, S. W. Robey, and D. A. Shirley, Phys. Rev. B **34**, 778 (1986).
[22]J. B. Pendry, *Low Energy Electron Diffraction* (Academic, London, 1974).
[23]V. Moruzzi, J. Janak, and A. Williams, *Calculated Electronic Properties of Metals* (Pergamon, New York, 1978).
[24]S. W. Robey, J. J. Barton, C. C. Bahr, G. Liu, and D. A. Shirley, Phys. Rev. B **35**, 1108 (1987).
[25]P. R. Bevington, *Data Reduction and Error Analysis for the Physical Sciences* (McGraw-Hill, New York, 1969).
[26]Y. K. Wu and K. A. R. Mitchell, Can. J. Chem. **67**, 1975 (1989).
[27]A. E. Schach von Wittenau, L. Q. Wang, Z. Hussain, Z. Q. Huang, and D. A. Shirley (unpublished).
[28]T. Yokoyama, M. Funabashi, Y. Kitajima, T. Ohta, and H. Kuroda, Physica B **158**, 643 (1989).
[29]U. Starke, F. Bothe, W. Oed, and K. Heinz, Surf. Sci. **232**, 56 (1990).
[30]J. Stohr, R. Jaeger, and S. Brennan, Surf. Sci. **117**, 503 (1982).
[31]R. D. Diehl (private communication).
[32]C. Kittel, *Introduction to Solid State Physics,* 6th ed. (Wiley, New York, 1986), p. 77.